Helium atom scattering study of the surface structure and dynamics of *in situ* cleaved MgO(001) single crystals

G. Benedek,* G. Brusdeylins, V. Senz, J. G. Skofronick,† J. P. Toennies, F. Traeger, and R. Vollmer
Max-Planck-Institut für Strömungsforschung, Bunsenstrasse 10, D-37073 Göttingen, Germany
(Received 12 February 2001; published 11 September 2001)

A high-resolution helium-atom scattering study on the surface structure and dynamics of *in situ* cleaved MgO(001) single crystals has been performed under ultrahigh vacuum conditions, in both high symmetry directions. Refined bound state resonance information is given for the energy levels of the He-MgO(001) surface potential, including confirmation of the lowest level at ~ -10 meV. A weak half-order reconstruction has been observed in diffraction scans in the $\langle 100 \rangle$ direction which is interpreted as due to a defect-induced release of the compressional surface stress. The Rayleigh modes were observed over most of the reduced surface Brillouin zone and found to agree with previous measurements and theory. At the zone boundaries the Rayleigh wave is no longer observed being replaced in the inelastic HAS spectrum by the first observations of the longitudinal Lucas mode and the crossing mode, both in agreement with given theoretical arguments.

DOI: 10.1103/PhysRevB.64.125421 PACS number(s): 68.35.Bs, 68.35.Ja, 63.20.Dj, 34.50.Dy

I. INTRODUCTION

The surface of monocrystalline magnesium oxide has acquired a considerable importance as a substrate for the growth of various materials because of its high melting and Debye temperatures. Due to its refractory material properties, the MgO surface is also used as a catalyst support. Moreover surface defects make the MgO surface useful as a heterogeneous catalyst which promotes the activation of methane for its partial oxidation process.[1,2] For these technological reasons and fundamental interests in the properties of metal oxides, the (001) surface of MgO has been the object of several experimental studies by means of helium atom scattering (HAS) addressing both the structural[3–6] and vibrational[3,6–9] properties. Similar studies have been carried out with low-energy electron diffraction (LEED) (Refs. 10 and 11) and electron energy-loss spectroscopy (EELS).[12] The early study of the excess phonon spectrum by neutron scattering from powders is also worth mentioning.[13] The electronic configuration and the surface stability of MgO have intrigued theorists due to the fact that the O^{2-} ion only exists in the condensed phase as an effect of crystal field stabilization and is expected to have a large polarizability at the surface where the coordination is reduced.[14] Such electronic effects may be held responsible for a compressional surface stress which affects the dispersion curves of surface phonons; for this reason the MgO surface has been studied theoretically for about three decades. The original effort was with rigid ion models,[15,16] followed by shell models of increasing complexity[17–23] and also the breathing shell model.[24]

In the early experimental work the samples were cleaved in air before being inserted into the vacuum system for HAS studies,[3,7] similarly to the successful procedure used for alkali halide surfaces.[3,25] For the air-cleaved alkali-halide samples a thermal treatment at several hundred degrees above room temperature in ultra high vacuum (UHV), where sublimation takes place, was used to produce a clean regular surface.[25] As observed later for NaCl samples baking the surface of samples cleaved *in situ* as well as *ex situ* to sublimation temperatures is not necessary and is conveniently replaced by simple annealing to about 400–500 K.[26,27] However, it became clear that cleaving *in situ* was indispensable for MgO studies[4–6,8–11,28] and desirable as well for alkali halide surfaces.

Early data for the air-cleaved MgO(001) surface[3] obtained at the Göttingen Max-Planck-Institut (MPI), despite our knowledge now of their lower quality, are nevertheless worth comparing to the vacuum-cleaved measurements reported by the Pennsylvania State University (PSU) group[4,5] and by us in the present paper. About ten years ago, an extended careful study using *in situ* cleaved MgO was undertaken by the PSU group using HAS. This work provided information on the surface structure and dynamics as well as on the surface bound states of ^{4}He.[4,5,8,9] The Rayleigh mode was measured up to nearly the surface Brillouin zone boundary for the $\langle 110 \rangle$ and to the boundary for the $\langle 100 \rangle$ directions. These measurements represented a major improvement, particularly for the surface dynamics, over the previous MPI data, likely due to a more sensitive instrument and the *in situ* cleaving. However, a disagreement remained over the lowest bound state at ~ -10 meV;[3,4,29] a situation similar to that of (Ref. 30) NaCl(001) which has been attributed to the different methods of measuring bound states. While the PSU group obtained bound state information by measuring the specular intensity as a function of the azimuth angle of the crystal, the MPI group obtained similar information from the angular distributions (ADs) as a function of the polar angle.[3] With the recent significant optimization of the MPI apparatus with regard to resolution and signal-to-noise ratio[31] a considerable amount of new information has been collected, by the different authors of this paper, in the last several years on the structure and dynamics of the MgO(001) surface.[32] These new features represent the main contributions reported in this paper.

The new results include (i) a confirmation of the previous deep bound state, (ii) a detailed measurement of the Rayleigh wave (RW) dispersion curves over much of the surface Brillouin zone, in agreement with the PSU work, (iii) the observation of high frequency modes at the zone boundaries above

the termination of the Rayleigh wave branch, and (iv) some evidence of a weak half-order reconstruction of the surface, presumably related to the occurrence of a strong surface stress and its release through surface defects.

In the next section the instrument is briefly described along with the measurement techniques. The results on the surface structure and dynamics are given in Secs. III and IV. A summary is given in the last section.

II. MEASUREMENT METHODS

Helium atom scattering from crystalline surfaces is now a well-documented method for surface studies.[8,25,31] For this reason, only a brief description of the instrument is given in this paper.

With respect to the original instrument decribed in Refs. 3,25 the new apparatus[31] works with the same 90°-scattering geometry, actually $\theta_i + \theta_f = 90.1°$ with θ_i and θ_f the incident and scattering angle, respectively. The angular resolution [full width half maximum (FWHM)] is 0.2°. In angular distribution measurements steps of 0.05° were used. The relative FWHM of the beam energy depends on the incident energy and is around 2% for the low-energy diffraction measurements shown here and 3.5% for the time-of-flight measurements.

All samples were prepared by mounting them onto a copper substrate attached to the manipulator, located inside of the UHV scattering chamber. The manipulator was baked at 150 °C and the vacuum chamber at 200 °C for 12–20 h. This provided a base pressure near 8.5×10^{-11} mbar.

The cleaving *in situ*, made at room temperature with the closing of two jaws on the sides of the crystal, nearly always produced a very high quality surface and no additional baking was necessary. In some cases, however, a slight misalignment of the jaws on the crystal might produce many steps on the surface yielding to a low-quality, poorly resolved inelastic structure between the main diffraction peaks. Actually, the quality of the surface could be monitored by the quality of the angular distributions.[25]

In most measurements of this work, the manipulator was that described in Refs. 31,32. In some measurements another manipulator was used, which was set up to reach surface temperatures as low as about 8 K and which allows only a poorer alignment of the crystal [see the difference in intensities of the Bragg peaks in Fig. 1 (b)]. The low-temperature studies were motivated by a renewed effort to understand the substrate prior to the adsorption studies of H_2 and N_2/MgO(001), work now in progress. Since the angular distributions are measured with the full helium-beam signal, a possible saturation of the electron multiplier in the magnetic mass sensitive detector was prevented by using a grid attenuator, when necessary. This guarantees an accurate determination of the peak FWHM.

The positions and intensities of specular and Bragg diffraction peaks in the ADs provide information on crystal surface periodicity and corrugation, respectively. Weaker minima and maxima, modulating the inelastic background between the diffraction peaks, are used to extract information on the bound states and surface reconstruction. Although some features of the AD like kinematical focussing (Ref. 33) (KF) and focussed inelastic resonances (Ref. 34) (FIR), carry some information on surface phonons, it is the time-of-flight (TOF) spectrum at different angles which provides the dynamics in the form of surface dispersion results. In TOF measurements, the beam is chopped into narrow pulses of 14 μs which collide with the crystal surface at a fixed incident angle θ_i. In inelastic collisions, the creation and annihilation of surface phonons cause the helium to lose or gain energy leading to longer or shorter flight times of the helium atoms, respectively, from the collision region to the detector at a distance of about 1 m. The TOF data for one phonon processes, used in conjunction with conservation of energy and momentum, yield the dispersion curves of surface phonons.[25]

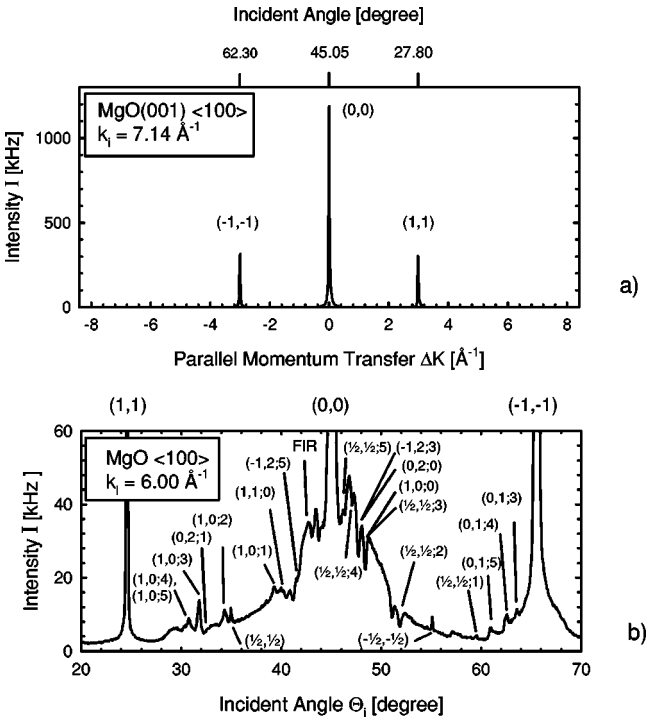

FIG. 1. (a) Plot of the scattered intensity as a function of parallel momentum transfer ΔK for the clean MgO(001) surface measured along the $\langle 100\rangle$ direction at an incident wave vector $k_i = 7.14$ Å^{-1} and a surface temperature of $T_S = 303$ K. (b) The structure in the background of another angular distribution measured at $k_i = 6.00$ Å^{-1} and $T_S = 307$ K plotted against incident angle θ_i and with an expanded intensity scale. The half-ordered peak which are due to the reconstruction are labeled with $(\pm\frac{1}{2}, \pm\frac{1}{2})$, bound state resonances are labeled according to the convention given in the text. In addition, on the basis of kinematics a feature is tentatively assigned to focussed inelastic resonances (FIR) involving (1,0;0).

III. STRUCTURE

A. Geometry and corrugation

Figures 1 and 2 show examples of angular distributions, namely the intensity of the reflected helium beam *versus* the

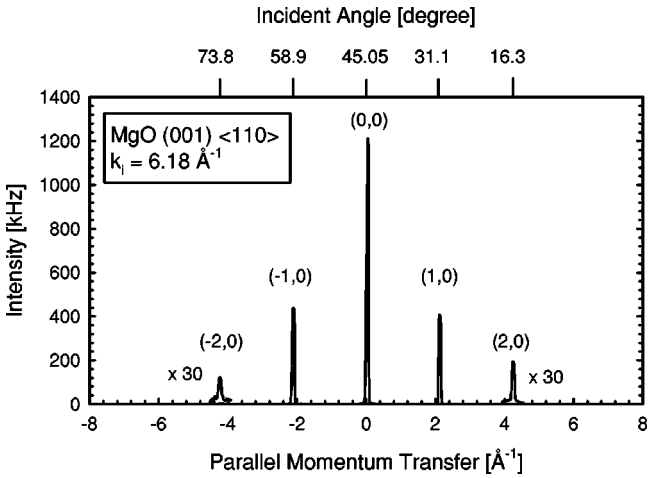

FIG. 2. Angular distribution along the $\langle 110\rangle$ of the MgO (001) surface measured at an incident wave vector of $k_i = 6.18$ Å^{-1} and a surface temperature of $T_S = 190$ K. The second order Bragg peaks are shown magnified by a factor of 30.

incident (polar) angle θ_i for the high symmetry directions $\langle 100\rangle$ and $\langle 110\rangle$. The measurements have been taken at surface temperatures and for incident wave vectors given in the captions. In Fig. 1 the ADs are displayed at two different scales in order to show the diffraction amplitudes (a) as well as the inelastic background (b), which exhibits a complex structure. Much of this structure can be analyzed in terms of bound-state resonances, from which the energy levels of the laterally averaged He-MgO(001) potential can be obtained. Another feature corresponds to the well-known (Refs. 33,34) FIR effect and one of the two minima at about 51° could be assigned to final state resonances.[35] Moreover, at the midpoints between the diffraction peaks (at 35° and 55°) in the $\langle 100\rangle$ direction there are additional narrow elastic peaks which are attributed to a weak reconstruction.

The positions of the integer-order Bragg peaks lead to the surface cell geometry which agrees with the bulk cell dimensions of 4.21 Å, whereas their amplitudes, analyzed within the eikonal approximation, lead to the corrugation.[32,36] The corrugation functional form has been adopted:

$$\zeta(x,y) = \frac{\zeta_0}{2}\left[\cos\left(\frac{2\pi x}{a}\right) + \cos\left(\frac{2\pi y}{a}\right)\right], \qquad (1)$$

where ζ_0 is the corrugation amplitude and $a = 2.98$ Å the surface cell size. The scattering intensities of the specular and Bragg peaks are calculated using the eikonal method and compared to the results from the experiment. The well depth of the He-MgO potential is taken into account using the Beeby correction.

The corrugation obtained from the data along $\langle 100\rangle$ is $\zeta_0 = 0.16 \pm 0.005$ Å, whereas the data along $\langle 110\rangle$ (Fig. 2) yield $\zeta_0 = 0.14 \pm 0.02$ Å. The error indicates the range of corrugation amplitudes obtained for different incident energies. We assume the systematical error of misalignment or of the averaging over directly and resonantly scattered intensity to be much smaller. In the analysis only well balanced angular distributions were used and the average calculated of the intensities of (n,m) and $(-n,-m)$ peaks, which usually differ in case of bad alignment. The contribution of resonantly scattered intensity to the measured total intensity is neglectable, it is at most in the range of tenth of percent. In Table I these values are compared to previous measurements. A new analysis of the data shown in Ref. 3 results in a corrugation amplitude of 0.16 Å and not 0.23 Å as stated there. Therefore the new value is reported in Table I.

There is good agreement between the present data and previous measurements[9,37] based on vacuum-cleaved crystals, as well as one of the studies based on air-cleaved crystals,[3] whereas the other data from air-cleaved crystals[7] yield a of about 0.07 Å larger value of ζ_0. Since the experimental conditions vary between the different experiments, it can only be speculated that the variations result from different surface qualities or heat treatments.

It is interesting to note that the measured corrugation is about the value that *ab initio* calculations by Li *et al.*[38] give at an electron density of 10^{-3} a.u. However, at the experimental incident energies the turning point for the He atoms is located where the electron density is about 10^{-4} a.u. The corrugation which would be obtained from an extrapolation of Li *et al. ab initio* results down to an electron density of 10^{-4} a.u. would probably be smaller than the experimental value.

B. Reconstruction

Between the large specular and Bragg peaks along the $\langle 100\rangle$ direction [Fig. 1(b)] the expanded intensity scale of the scattered intensity shows a fine structure with numerous

TABLE I. The corrugation amplitude of the MgO(001) surface as obtained from different He-atom scattering experiments.

Corrugation amplitude ζ_0 (Å)	Incident energy E_i(meV)	Well depth D(meV)	Reference
0.16 ± 0.01	20	12.5	Brusdeylins *et al.* (Ref. 3)
0.235 ± 0.01	~ 67	8	Cantini *et al.* (Ref. 7)
0.17 ± 0.03	17.3–63	7.5	Jung *et al.* (Ref. 9)
0.18 ± 0.02	63–86	not taken into account	Rieder (Ref. 37)
0.19	19.6	not taken into account	Fahsold *et al.* (Ref. 6)
0.14 ± 0.02	13–58	12.5	this work $\langle 110\rangle$
0.16 ± 0.005	27–60	12.5	this work $\langle 100\rangle$

maxima and minima. The structure falls into two categories: (i) the additional half-integer diffraction peaks which indicate a weak reconstruction and (ii) the resonance phenomena, which will be covered in the next subsection.

Half-integer diffraction peaks have been observed along the $\langle 100 \rangle$ direction in a significant number of cleaved MgO surfaces.[32] An example is given in Fig. 1(b), where a pair of weak, very sharp peaks marked $(\pm\frac{1}{2},\pm\frac{1}{2})$ occur half-way between the specular and the Bragg peaks. However, it is difficult to derive from these features a quantitative information on the structure of the reconstructed phase. Actually we have observed that the scattering intensity of the additional peaks changes from one sample to another and even varies on different spots of the same crystal surface: the additional peaks may not be seen at all or show a few kHz of He count rate. The latter fact suggests the presence of reconstructed domains distributed over the (001) surface. The areal size of the domains may well be in the 100-nanometric scale, but larger than the coherence length of the He beam, which is in the range of about 200–400 Å. This can be inferred from the fact that observed half-order diffraction peaks are not broadened.

A reconstruction of the (001) surface of ionic crystals with the rocksalt structure is rather unusual, although a probably different kind of reconstruction has been observed in AgBr(001) and, occasionally, even in NaCl(001).[39] While in AgBr(001) the reconstruction could clearly be explained as an ordering of defects at the surface, the weak, erratic $(\sqrt{2}\times\sqrt{2})$ reconstruction on MgO(001) may also have its origin in the presence of surface defects, e.g., anion vacancies, though at low concentration.

The MgO(001) surface is characterized by a comparatively strong compressional surface stress. This can be seen from a relationship existing, for the rocksalt (001) surface, between the surface stress and the dispersion of the shear Lucas (S_5) mode in the $\bar{\Gamma}\bar{M}$ direction.[40] Shell model calculations of the surface phonon dispersion curves[17,23] clearly show for MgO(001) a fairly large upward dispersion of the S_5 mode from $\bar{\Gamma}$ to $\bar{M}$, as compared, e.g., to that of alkali halides. Surface defects may trigger a release of the surface stress through a reconstruction over certain domains, the size of which may depend on defect concentration. A soft-mode mechanism for the $(\sqrt{2}\times\sqrt{2})$ reconstruction in the (001) surface of rocksalt ionic crystals with a large difference in the ionic radii of the two ionic species has been suggested long ago on the basis of the breathing shell model.[41] The ionic size difference produces a large compressive surface stress which is accommodated by a rumpling of the oxygen surface sublattice.

C. Bound state resonances and energy levels

Most of the other observed features in the AD shown in Fig. 1(b) between diffraction peaks can be ascribed to bound-state resonances. A simple kinematic relation, based on energy conservation, links the incident energy E_i and incident parallel momentum $\mathbf{K}_i$ to a bound state energy $-|e_j|$:

TABLE II. A compilation of bound states of the He-MgO(001) potential obtained from different He-atom scattering experiments.

Bound state $-\lvert e_j\rvert$ [meV]	Ref. 4	Ref. 3	This work
$-\lvert e_0\rvert$		−10.2	−10.2
$-\lvert e_1\rvert$	−5.52	−6.0	−5.3
$-\lvert e_2\rvert$	−2.57	−2.6	−2.4
$-\lvert e_3\rvert$	−1.16	−1.2	−0.90
$-\lvert e_4\rvert$	−0.54		−0.55
$-\lvert e_5\rvert$	−0.26		−0.20

$$(\mathbf{K}_i+\mathbf{G}_{mn})^2=\frac{2m}{\hbar^2}(E_i+|e_j|), \tag{2}$$

where $\mathbf{G}_{mn}$ is a surface reciprocal lattice vector. Since $K_i=k_i\cdot\sin\theta_i$, Eq. (2) gives the incident angle θ_i (if any) at which a resonance with the bound state of energy $-|e_j|$ occurs through the exchange of a G vector $\mathbf{G}_{mn}$. Thus each resonance is labeled by $(m,n;j)$ [Fig. 1(b)]. As pointed out by Miret-Artés,[42,43] and references therein, the shape of the resonance may be a single Lorentzian minimum or maximum or a Fano-type feature depending on the potential function and the surface temperature. Thus the identification of resonance features in the angular distributions needs some care. Figure 1(b) shows the assignment of peaks in an angular distribution at the incident wave vector of 6.00 Å^{-1}. The experimental error of the determination of bound state energies is about ± 0.1 meV. The energies of the five lowest bound states $|e_j|$ ($j=$ 0 to 5), are listed in Table II and compared with previous measurements with comparable incident wave vectors. In Table II, this work has six, whereas the PSU work[4] has five levels. The lowest level $e_0=-10.2$ meV, previously found in air-cleaved samples from resonances in the angular distribution,[3] is here confirmed, whereas the specular intensity measurements in vacuum-cleaved samples, where the azimuth angle was varied, did not show this level.[4,8,9] Such discrepancy between deep-level resonances observed in the inelastic background of angular distributions and those derived from specular intensity oscillations was already observed in NaCl (001) (Ref. 30) and explained as due to the larger probability of inelastic processes for atoms trapped in the lowest bound states.

By assuming a 9-3 Lennard-Jones form for the G=0 component of the surface potential,[44] the bound state energies can be expressed in the WKB approximation as[44]

$$|e_j|_{\text{WKB}}=-D\left(1-\frac{\pi\hbar}{3.07}\frac{j+1/2}{\sigma(2mD)^{1/2}}\right)^6. \tag{3}$$

D and σ are the depth and the vanishing point of the Lennard-Jones potential. Equation (3) provides a fairly good fit of the experimental energy levels with $D=(13.8\pm 0.4)$ meV and $\sigma=(2.03\pm 0.15)$ Å.

IV. SURFACE PHONON DISPERSION CURVES

The insets in Figs. 3 and 4 show two TOF spectra (converted into an energy-transfer scale) taken along the two

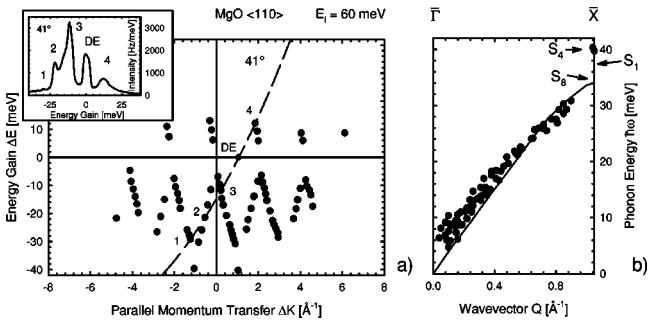

FIG. 3. (a) Plot of energy gain vs the parallel momentum transfer in the $\langle 110\rangle$ direction for an incident energy of 60 meV as derived from the inelastic peaks of TOF spectra. The experimental points 1–4 alligned on the scan curve for $\Theta_i = 41°$ are associated with four peaks in the corresponding TOF spectrum shown in the inset after conversion to the energy transfer scale. The diffuse elastic peak which results from incoherent scattering from surface defects is labeled "DE." This measurement was taken at a surface temperature of $T_S = 300$ K. (b) The experimental points folded back into the reduced surface Brillouin zone in the positive quadrant of the $(\Delta K, \Delta E)$ plot give the phonon energy $\overline{\hbar\omega}$ as a function of the phonon wave vector $\vec{Q}$. The theoretical energies of the Rayleigh (S_1), crossing (S_8), and Lucas (S_4) phonons at the zone boundary $\overline{X}$ point are indicated by arrows. At $\overline{X}$ the scattering intensity of the Rayleigh wave is transferred to the optical Lucas mode.

high-symmetry directions at a given incident angle. Many such spectra have been measured at different incident angles. The energy gains (creation events) and losses (annihilation events) corresponding to the peaks in the TOF spectra are plotted as a function of the corresponding parallel momentum transfer in Figs. 3 and 4 (left). The experimental data span several surface Brillouin zones on both the creation and the annihilation sides. When these data are folded back into the first Brillouin zone, the phonon dispersion curves are obtained (full circles in Figs. 3 and 4, right) and directly compared to the original theoretical calculation (full lines)[18] by Chen *et al.*

There is very good agreement with the theoretical dispersion curves of the Rayleigh wave (here labeled S_1 for both directions according to the labeling rules defined in Refs. 45,40) and with previous measurements,[3–5] except near the

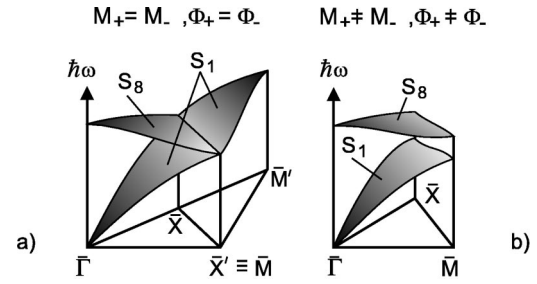

FIG. 5. Dispersion relation of the Rayleigh wave (S_1) of a diatomic lattice with the rocksalt structure when the ionic masses and interactions are identical for the two ions and can therefore be considered to form a monoatomic lattice with a doubled Brillouin zone (a), and when the ionic masses and/or interactions are slightly different (b); the folding of the Rayleigh mode branch into the reduced Brillouin zone of the diatomic lattice gives rise to the crossing mode branch S_8.

zone boundary, where the present high-resolution measurements reveal a more complex situation, which is discussed below. At small wave vectors there is an apparent shift of the HAS experimental points from the Rayleigh wave (RW) dispersion curve towards the bulk continuum. This is sometimes observed in HAS (Ref. 25) when the RW signal becomes weak as compared to that of the bulk modes and its FWHM is comparable, in the momentum space, to the parallel momentum transfer.

At the zone boundaries MgO(001) exhibits the typical behavior of a diatomic crystal with nearly equal atomic masses, e.g., NaF(001).[46] This is illustrated in Fig. 5. If the ionic masses and the forces acting on the two ions were identical (as would happen in a rigid-ion model, with only Coulomb and nearest-neighbor repulsive interactions), the diatomic rocksalt crystal would be indistinguishable from a monoatomic simple cubic crystal. If viewed as a monoatomic crystal, its RW dispersion curve S_1 would extend over the Brillouin zone $\overline{\Gamma X' M'}$ [Fig. 5(a)], which is twice that for the diatomic crystal where its RW dispersion curve is folded back into the reduced zone $\overline{\Gamma M X}$, and we have therefore two branches S_1 and S_8, the latter being called the "crossing mode" or "crossing resonance" as it cuts the continuum of the bulk modes.[45,46] When the ionic masses and/or the interactions of the two ions are different, a gap opens between the

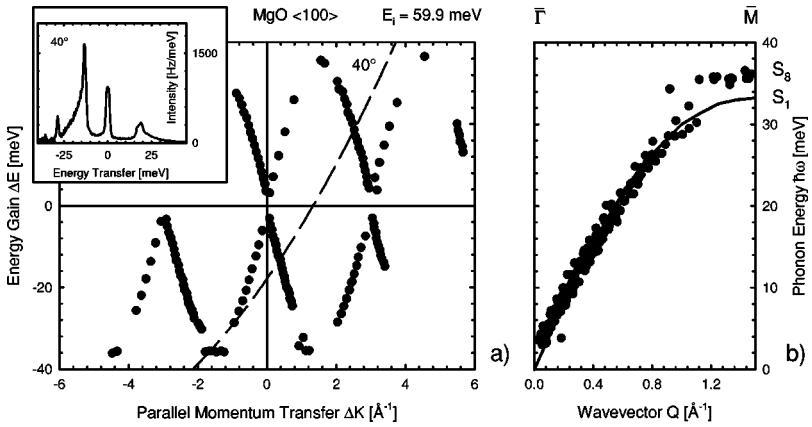

FIG. 4. The same as Fig. 3 for the $\langle 100\rangle$ direction at a surface temperature of $T_S = 304$ K and $E_i = 59.9$ meV. The scan curve and the TOF spectrum in the inset correspond to $\Theta_i = 40°$. The phonon dispersion curves appearing in the folded plot (b) show in this case a transfer of scattering intensity from the Rayleigh (S_1) to the crossing (S_8) mode at the zone boundary $(\overline{M}$ point).

two branches. In the Chen *et al.*calculation,[17,23] the S_8 mode (called S_6 in that paper) is interchanged with the RW at the $\overline{X}$ point. It should be noted that at the zone boundary only the heavier ion (Mg^{2+}) is moving for the S_1 mode, whereas the lighter ion (O^{2-}) moves alone in the S_8 mode. Since the Mg^{2+} ion is very small, its motion is weakly coupled to the He atom and therefore the scattering intensity switches from S_1 to S_8 when approaching the zone boundary (Fig. 4). This effect was not noticed in previous measurements presumably due to poorer resolution. At the $\overline{X}$ point two high frequency data points are seen to correspond to the optical surface mode with longitudinal polarization (the Lucas mode S_4) (Fig. 3). Near the $\overline{M}$ region, the scattering intensity switches from the Rayleigh mode S_1 to the S_8 crossing mode (Fig. 4) as discussed with Fig. 5.

V. SUMMARY

In this article a summary of helium atom scattering measurements of the structure and dynamics the MgO(001) surface is presented. In diffraction experiments the predominant part of the surface shows the symmetry expected for the rocksalt structure with a corrugation amplitude of 0.14–0.16 Å, which is in reasonable agreement with reported results.

Regarding the structure, the primary result of this work is the identification of a weak half-order reconstruction on parts of the MgO(001) surface. A possible mechanism leading to a $(\sqrt{2}\times\sqrt{2})$ reconstruction is given, which is based on the presence of large compressive surface stress and a certain amount of surface defects. The surface stress is caused by the difference in size between the surface ions and its presence is theoretically confirmed by the dispersion of the S_5 mode in the calculations of Refs. 17,23.

The determined bound states of the laterally averaged He-MgO potential confirm the three lower bound states (e_{0-2}) reported previously by our group. Corrected values for e_3 and e_5 are also provided. The bound energy at -10.15 meV has not been seen in other experiments.[4] This is a second example for the observation that the peaks in the ADs are somewhat more sensitive to the lowest energy bound state than the method of azimuthal scans. However, the combined data in Table II does suggest the existence of an additional bound state.

For the Rayleigh mode, the surface dispersion curve agrees with both theory and previous measurements. In addition, close to the $\overline{M}$ point the crossing mode S_8 is observed. At that point it is related to the motion of the lighter oxygen ion and because the oxygen ion has a larger ionic radius than the Mg ionic radius, it therefore couples more strongly to the scattered He atoms than the Rayleigh wave. At the $\overline{X}$ point there is some evidence for the Lucas mode S_4.

ACKNOWLEDGMENTS

This research was supported in part (JGS) by DOE Grant No. DE-FG02-97ER45635. He thanks Professor J. P. Toennies and the Max-Planck-Institut für Strömungsforschung for their hospitality during part of this work and also Dr. S. Miret-Artés and E. Akhadov for help with the manuscript.

*Also at: Istituto Nazionale per la Fisica della Materia, Dipartimento di Scienza dei Materiali, Università di Milano-Bicocca, via Cozzi 53, I-20125 Milano, Italy

†Also at: Department of Physics and MARTECH, Florida State University, Tallahassee, Florida 32306, USA,

[1] A. D'Ercole and C. Pisani, J. Chem. Phys. **111**, 9743 (1999).
[2] K. Hermansson, M. Baudin, B. Ensing, M. Alfredsson, and M. Wojcik, J. Chem. Phys. **109**, 7515 (1998).
[3] G. Brusdeylins, R.B. Doak, J.G. Skofronick, and J.P. Toennies, Surf. Sci. **128**, 191 (1983).
[4] M. Mahgerefteh, D.R. Jung, and D.R. Frankl, Phys. Rev. B **39**, 3900 (1989).
[5] David R. Jung, M. Mahgerefteh, and D.R. Frankl, Phys. Rev. B **39**, 11 164 (1989).
[6] G. Fahsold, G. König, W. Theis, A. Lehmann, and K.-H. Rieder, Appl. Surf. Sci. **137**, 224 (1999).
[7] P. Cantini and E. Cevasco, Surf. Sci. **148**, 37 (1984).
[8] J. Cui, D.R. Jung, and D.R. Frankl, Phys. Rev. B **42**, 9701 (1990).
[9] D.R. Jung, J. Cui, and D.R. Frankl, J. Vac. Sci. Technol. A **9**, 1589 (1991).
[10] D.L. Blanchard, D.L. Lessor, J.P. LaFemina, D.R. Baer, W.K. Ford, and T. Guo, J. Vac. Sci. Technol. A **9**, 1814 (1991).
[11] T. Urano, T. Kanaji, and M. Kaburagi, Surf. Sci. **134**, 109 (1983).
[12] C. Oshima, T. Aizawa, R. Souda, and Y. Ishizawa, Solid State Commun. **73**, 731 (1990).
[13] K.H. Rieder and E.M. Hörl, Phys. Rev. Lett. **20**, 209 (1968).
[14] A.J. Martin and H. Bilz, Phys. Rev. B **19**, 6593 (1979).
[15] L. Genzel and T.P. Martin, Phys. Status Solidi A **51**, 101 (1972).
[16] G. Lakshmi and F.W. de Wette, Phys. Rev. B **22**, 5009 (1980).
[17] T.S. Chen, G.P. Alldredge, and F.W. de Wette, Phys. Lett. **46A**, 91 (1973).
[18] T.S. Chen, F.W. de Wette, and G.P. Alldredge, Phys. Rev. B **15**, 1167 (1977).
[19] G. Laksmi and F.W. de Wette, Phys. Rev. B **23**, 2035 (1981).
[20] P.A. Maksym, Surf. Sci. **149**, 157 (1985).
[21] F.W. de Wette, W. Kress, and U. Schröder, Phys. Rev. B **32**, 4143 (1985).
[22] W. Kress, F.W. de Wette, A.D. Kulkarni, and U. Schröder, Phys. Rev. B **35**, 5783 (1987).
[23] F.W. de Wette, in *Surface Phonons*, edited by W. Kress and F.W. de Wette (Springer Verlag, Heidelberg, 1991), p. 67.
[24] R.N. Barnett and R. Bass, Phys. Rev. B **19**, 4259 (1979).
[25] G. Brusdeylins, R.B. Doak, and J.P. Toennies, Phys. Rev. B **27**, 3662 (1983).
[26] A.L. Glebov, J.P. Toennies, J.G. Skofronick, and J.R. Manson, Phys. Rev. B **58**, 10012 (1998).
[27] J. G. Skofronick, F. Traeger, J. P. Toennies, and H. Weiss (unpublished).
[28] C. Duriez, C. Chapon, C.R. Henry, and J.M. Rickard, Surf. Sci. **230**, 123 (1990).
[29] M. Karimi and G. Vidali, Phys. Rev. B **39**, 3854 (1989).
[30] G. Benedek, A. Glebov, W. Silvestri, J.G. Skofronick, and J.P. Toennies, Surf. Sci. **381**, L540 (1997); **406**, L621 (1998).
[31] J.P. Toennies and R. Vollmer, Phys. Rev. B **44**, 9833 (1991).

[32] V. Senz, Diploma thesis, Georg August Universität, Göttingen, 1996; R. Gerlach and F. Traeger (unpublished).
[33] G. Benedek, Phys. Rev. Lett. **35**, 234 (1975).
[34] G. Benedek and S. Miret-Artés, Surf. Sci. Lett. **339**, 935 (1995).
[35] G. Benedek, J. P. Toennies, and F. Traeger (unpublished).
[36] U. Garibaldi, A.C. Levi, R. Spadacini, and G.E. Tommei, Surf. Sci. **48**, 649 (1975).
[37] K.H. Rieder, Surf. Sci. **118**, 57 (1982).
[38] Ye Li, D.C. Langreth, and M. Pederson, Phys. Rev. B **55**, 16 456 (1997).
[39] A.L. Glebov, J.P. Toennies, and F. Traeger, Phys. Rev. Lett. **82**, 4492 (1999).
[40] J.P. Toennies and G. Benedek (unpublished). Unfortunately, the dispersion of the shear-horizontal Lucas mode (S_5) could not be measured yet.
[41] G. Benedek, *Atomic Structure and Mechanical Properties of Metals*, edited by J. Bilello and G. Caglioti (Varenna, Compositori Bologna, 1976), p. 516.
[42] S. Miret-Artés, Surf. Sci. Lett. **339**, 205 (1995).
[43] S. Miret-Artés, Surf. Sci. Lett. **366**, 735 (1996).
[44] M.W. Cole and T.T. Tsong, Surf. Sci. **69**, 325 (1977).
[45] G. Benedek and L. Miglio, in *Surface Phonons*, edited by W. Kress and F.W. de Wette (Springer Verlag, Berlin, 1991), p. 37.
[46] G. Benedek, L. Miglio, G. Brusdeylins, J.G. Skofronick, and J.P. Toennies, Phys. Rev. B **35**, 6593 (1987).